Journal of Directed Energy, **1**, Spring 2004, 93–109

Superheating and Material Ablation of Metals by Multiple Ultrashort Laser Pulses

J. K. Chen* **and J. E. Beraun**

Laser Effects Research Branch, Directed Energy Directorate, Air Force Research Laboratory, Kirtland Air Force Base, New Mexico 87117

For metals and metal-like materials subjected to high-power ultrashort-pulse laser heating, phase explosion is believed to be a dominating mechanism that sputters the material away. The two-step heating equations along with an isothermal solid–liquid phase transformation are proposed to evaluate the amount of ablated material by ultrafast lasers. Numerical analysis is performed for gold films in vacuum irradiated by an ultrashort UV laser. When the superheated liquid temperature at a grid point reaches $0.9T_{tc}$ *(T_{tc} denoting the thermodynamic equilibrium critical temperature), phase explosion is assumed and the grid point is thus removed. The calculated ablation depth matches well with experimental data. It is found that two consecutive pulses split from a high-power, ultrashort-pulse laser beam could ablate more material than the single beam if the first pulse fluence is greater than the ablation threshold.*

KEYWORDS: Laser ablation, Phase explosion, Superheating, Ultrashort-pulsed laser

Nomenclature

A_e, B_l	material constants in electron relaxation time
C	bulk heat capacity
C_e	electron heat capacity
C_{eo}	material constant in electron heat capacity
C_l	lattice heat capacity
C_{pb}	specific heat at T_b
E	Young's modulus
G	electron–phonon coupling factor
H_m	fusion latent heat
J_o	fluence of a single laser pulse
J_{oi}	fluence of the ith laser pulse
J_{sh}	ablation threshold fluence
K_e	electron thermal conductivity
K_l	lattice thermal conductivity
L	current film thickness
L_o	initial film thickness

Received January 29, 2003; revision received May 29, 2003.

*Corresponding author.

N	total number of laser pulses
q_e	heat flux in electron gas
q_l	heat flux in a lattice
R_i	surface reflectivity
S_i	ith volumetric laser heat source
T	temperature
T_b	normal boiling temperature
T_e	electron temperature
T_F	Fermi temperature
T_l	lattice temperature
T_m	melting temperature
T_o	initial (reference) temperature
T_{tc}	thermodynamic equilibrium critical temperature
t	time
t_{ml}	time when solid–liquid phase change ends
t_{ms}	time when solid–liquid phase change starts
t_p	width of a single laser pulse at half-maximum intensity
t_{pi}	width of the ith laser pulse at half-maximum intensity
t_{pki}	time when the ith laser pulse reaches the peak power
u	unit step function
V_s	speed of sound
x	spatial coordinate
β	4ln(2), a constant
Δt	separation time between two pulses
χ, η	material constants in electron thermal conductivity
ϕ_e	T_e/T_F, normalized electron temperature
ϕ_l	T_l/T_F, normalized lattice temperature
λ	laser wavelength
ν	Poisson's ratio
ρ	mass density
ρ_b	mass density at T_b
τ_e	electron relaxation time
τ_l	phonon relaxation time

1. Introduction

The rapid development of femtosecond lasers over the past decade has opened up a wide range of new applications in physics, chemistry, material science, and medicine. For material processing, for instance, ultrashort-pulse lasers have advantages over conventional pulse lasers, such as 1) ultrahigh precision, 2) minimal collateral thermal damage, 3) large material removal rate, and 4) the capability of processing practically any material (Refs. 20, 21, 24, and 26, for example). To control and optimize the ultrashort laser material processing, an understanding of thermal transport in and material ablation from a solid target is of importance.

Phase explosion (or termed explosive boiling) was first proposed by Martynyuk[17] in 1974 for discharging a condensor into a wire. An important argument to the high-power, very short (<1-ns) pulse laser heating was made some 20 years later.[14,15,19] Recently, experimental observation of phase explosion of materials by short-pulse lasers has been reported.[9–11,25,27,34]

For metals and metal-like materials subjected to high-power, ultrashort-pulse laser heating, a melted material at and beneath the irradiated surface, according to Kelly and Miotello,[14] is unable to boil because the time scale does not permit the necessary heterogeneous nuclei to form. Instead, the melted material is superheated significantly past the normal boiling point T_b to more or less the limit T_{tc} (the thermodynamic equilibrium critical temperature). The tensile strength of the superheated (metastable) liquid falls to zero; moreover, fluctuation in volume becomes drastic, especially near the critical temperature T_{tc}. Consequently, homogeneous bubble nucleation occurs at an extremely high rate. For instance, the rate of homogeneous nucleation for cesium (Cs) are 1 $cm^{-3}s^{-1}$ at $T = 0.874T_{tc}$ and 10^{26} $cm^{-3}s^{-1}$ at $T = 0.905T_{tc}$ (Ref. 18). As a result of the tremendous number of homogeneous nuclei rapidly formed, the near-surface region of the irradiated material relaxes explosively (or sputters) into a mixture of vapor and equilibrium liquid droplets that are immediately ejected from the bulk material.

Numerous theoretical investigations on phase explosion by short-pulse lasers have been reported recently.[3,4,6,12,16,23,32,33] Bulgakova and Bulgakov,[4] Lu et al.,[16] Willis and Xu,[32] and Xu et al.[33] used the classical thermal approach to evaluate the ablation rate and surface temperature for laser pulses of several-tens of picoseconds and longer. Bulgakova and Bourakov[3] employed a two-temperature thermal model along with Euler equations for the vapor layer to investigate the possibility of phase explosion. Schäfer and Urbassek[23] combined a hybrid finite difference and molecule dynamics analysis for subpicosecond laser ablation of copper. Based on the force that the electric field of charge separation pulls the ions out of a target, Gamaly et al.[12] derived the analytical formulas for the ablation threshold and ablation depth for metals and dielectrics irradiated by ultrashort-pulse lasers with an intensity in the range of 10^{13}–10^{14} W/cm^2. Chen and Beraun[6] found that in spite of the fact that each of the two properties changes drastically with temperature, the product of specific heat C_p and mass density ρ for a liquid metal remains fairly constant up to the point near $0.9T_{tc}$ (Fig. 1). Thus, the total heat absorbed by a material point from T_b to $0.9T_{tc}$

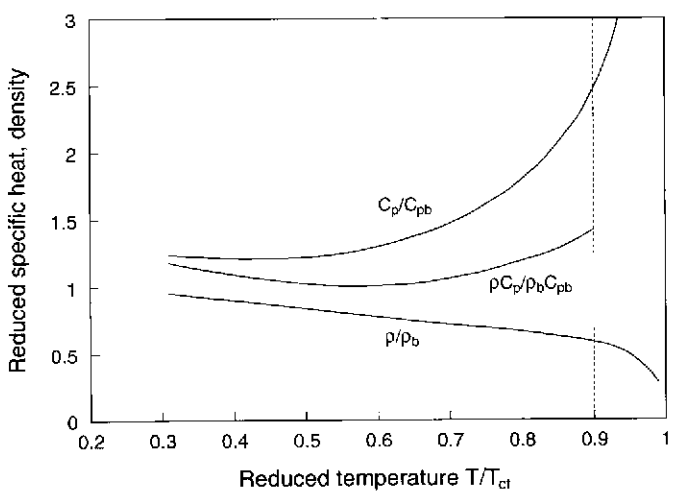

Fig. 1. Typical variations of specific heat C_p and mass density ρ beyond the normal boiling temperature for a liquid metal. The subscript b denotes properties at the normal boiling point.

can be approximated by

$$\int_{T_b}^{0.9T_{tc}} \rho C_p \, dT \sim \rho_b C_{pb}(0.9T_{tc} - T_b). \tag{1}$$

By assuming that the heat capacity beyond the normal boiling point is constant and equals $\rho_b C_{pb}$, Chen and Beraun[6] simulated the superheating up to $0.9T_{tc}$, a critical temperature that phase explosion takes place.[14,15,17–19] The ablation threshold J_{sh} for gold films in vacuum irradiated by a subpicosecond UV laser they calculated is 0.244 J/m^2, which is close to the measurement ~0.17 J/cm^2 (Ref. 21). In addition, their calculation of the ablation depth correlates well with the experimental data for laser fluences higher than 0.27 J/cm^2 (Ref. 21).

In this paper, the two-step heating equations[5,22] along with an isothermal solid–liquid phase change[13] are proposed to model the superheating in and the material ablation from metal materials caused by multiple ultashort laser pulses based on the concept of phase explosion. The coupled, nonlinear partial differential equations for the temperatures in the two subsystems (electrons and lattice) are solved with a finite difference method. Numerical analysis is performed for gold films in vacuum heated by an ultrashort UV laser. When the superheated liquid temperature at a grid point is equal to or greater than $0.9T_{tc}$, phase explosion is assumed. The grid point, containing both the electrons and the superheated liquid, that undergoes the phase explosion as well as the associated thermal energy are then removed. Numerical results, including the electron and lattice (phonon) temperature distributions, the time history of material loss, and the ablation depth as a function of laser fluence, are presented and discussed. In addition, the effects of laser pulse duration, film thickness, and multiple-pulse laser heating on the material ablation are investigated.

2. Mathematical Model

To investigate the emission of electrons from a metal surface exposed to an ultrashort laser pulse, Anisimov et al.[1] proposed a phenomenological two-temperature model that can describe the electron and lattice temperature fields. In the first step of their model, the incident laser energy is absorbed by the free electrons that are confined within the optical penetration depth (α) during the laser heating. In the second step, part of the electron thermal energy transfers to the lattice through the electron–phonon coupling and, in the meantime, part of the electron thermal energy diffuses into deeper regions of the material. By removing the assumption of instantaneous thermal equilibrium in electrons made in Ref. 1, Qiu and Tien[22] derived a more rigorous, two-step heating model from the Boltzmann transport equation. Accordingly, Qiu and Tien's theory is suitable for laser pulse lengths on the order of or shorter than the electron relaxation time. Chen and Beraun[5] extended Qiu and Tien's theory by introducing the thermal wave type of heat conduction in the lattice. To distinguish the above three two-temperature models, they are referred to be parabolic,[1] hyperbolic,[22] and dual hyperbolic.[5] In this work the dual-hyperbolic, two-temperature equations[5] together with the isothermal solid–liquid phase transformation,[14] for general purpose, are proposed to evaluate material ablation by multiple ultrafast laser pulses. Let the origin of the axis x locate at the back surface of a film target (Fig. 2). The one-dimensional (1D) form of the proposed ablation model is written as

$$C_e \frac{\partial T_e}{\partial t} = -\frac{\partial q_e}{\partial x} - G(T_e - T_l) + \sum_{i=1}^{N} S_i(x, t), \tag{2}$$

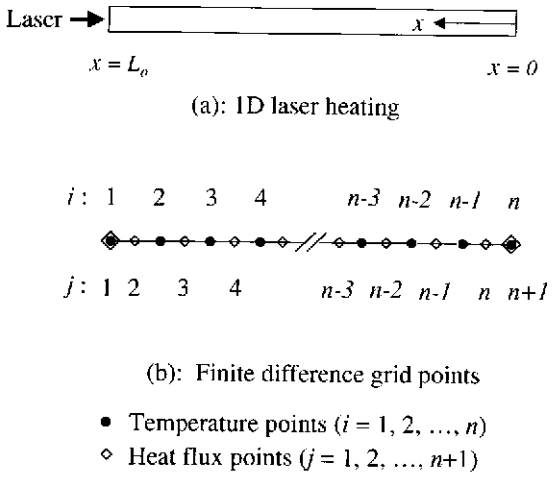

Fig. 2. Sketch of the 1D laser heating problem and the finite difference mesh.

$$\tau_e \frac{\partial q_e}{\partial t} + q_e = -K_e \frac{\partial T_e}{\partial x}, \tag{3}$$

$$C_l \frac{\partial T_l}{\partial t} = -\frac{\partial q_l}{\partial x} + G(T_e - T_l) \qquad (T_l \neq T_m), \tag{4}$$

$$\int_{t_{ms}}^{t_{ml}} \left[-\frac{\partial q_l}{\partial x} + G(T_e - T_l) \right] dt = \rho H_m \qquad (T_l = T_m), \tag{5}$$

$$\tau_l \frac{\partial q_l}{\partial t} + q_l = -K_l \frac{\partial T_l}{\partial x}. \tag{6}$$

The quantities with subscripts e and l are associated with electrons and the lattice, respectively. While melting ($T_l = T_m$), the lattice temperature remains unchanged until the solid–liquid phase transformation is completed. The start time t_{ms} of the phase transformation at a material point is determined by Eq. (4), and the end time t_{ml} is determined by Eq. (5). Since the rate of vapor loss from a metal material is very small,[17,32] surface vaporization due to normal boiling is neglected in the present model. For phase explosion to take place, the bubbles should reach a critical dimension before they can burst. To accurately describe the phase explosion, the kinetics of nucleus formation, the violent, explosive boiling mechanism, the stability of liquid droplets, the critical bubble radius for phase explosion, and the effects of the purity of material in the vicinity of the spinodal must be addressed. Since the detailed process that homogeneous and/or heterogeneous bubbles are formed and explode remains unsolved, it is not modeled here. Instead, phase explosion is simply assumed when the superheated liquid temperature at a grid point is equal to or greater than $0.9T_{tc}$. The grid point, containing the electrons and the superheated liquid, that undergoes the phase explosion as well as the associated thermal energy are then removed instantaneously.

The bulk thermal conductivity is the sum of the electronic component K_e and the lattice component K_l. For pure metals, K_e in general is much larger than K_l. Therefore, heat conduction in a pure metal lattice is often neglected.[1,22] In this case the gradient of heat flux ($\partial q_l / \partial x$) in Eq. (3) along with Eq. (4) is dropped off from the two-temperature model. For alloys and semiconductor materials, on the other hand, the contribution of K_l to K

is significant, and thus, heat conduction in the lattice should be retained. Because the electron–phonon thermalization time is shorter than phonon relaxation time, the Cattaneo–Vernotte constitutive equation (6) (Ref. 29) is coupled with the energy equation (4). The heat transport in the lattice described above is thus hyperbolic in general, which is different from the parabolic diffusion employing Fourier's law.

For a Gaussian laser pulse, the mathematical form of 1D volumetric laser heat sources S_i is expressed as

$$S_i(x,t) = \sqrt{\frac{\beta}{\pi}} \frac{(1-R_i)J_{oi}}{t_{pi}\alpha_i} \exp\left\{-\left[\frac{L(t)-x}{\alpha_i}\right] - \beta\left(\frac{t-t_{pki}}{t_{pi}}\right)^2\right\} \qquad (i = 1, 2, \ldots, N). \tag{7}$$

Equation (7) indicates that the laser pulses are aimed at the surface $x = L(t)$. As the depth increases, the intensity of the volumetric laser heat sources attenuates with the exponential function $\exp\{-[L(t) - x]/\alpha_i\}$. The peak laser powers occur at $t = t_{pki}$. For each pulse the lasing starts at $t = t_{pki} - 2t_{pi}$ and ends at $t = t_{pki} + 2t_{pi}$. The laser energy outside the period of the lasing time assumed here is very small and thus is neglected.

The governing equations (2)–(6) will be solved with proper initial and boundary conditions. For simplicity, the following conditions are considered:

$$T_e(x,0) = T_l(x,0) = T_o, \tag{8}$$

$$q_e(0,t) = q_e(L,t) = 0, \tag{9}$$

$$q_l(0,t) = q_l(L,t) = 0, \tag{10}$$

where the initial temperature T_o is set at 300 K (room temperature).

For ultrashort-pulse laser ablation, electron temperature induced in metals could be very high, on the order of the Fermi temperature T_F. Consequently, the thermophysical properties of electrons used in the model should be valid over a wide range of temperature. Among these properties, the electron heat capacity C_e is proportional to the electron temperature:

$$C_e = C_{eo}T_e. \tag{11}$$

Equation (11) is adequate as long as electron temperature is below T_F (Ref. 35). The electron thermal conductivity K_e is subjected to considerable uncertainty since it depends on the local electronic and atomic temperatures. A functional form for the electron thermal conductivity that has been employed for modeling ultrashort laser heating for temperatures over a range from room temperature to the Fermi temperature[2,6,23] is implemented:

$$K_e = \chi \frac{(\phi_e^2 + 0.16)^{5/4}(\phi_e^2 + 0.44)\phi_e}{(\phi_e^2 + 0.092)^{1/2}(\phi_e^2 + \eta\phi_l)}. \tag{12}$$

The electron relaxation time τ_e characterized in Ref. 31 is suitable for electron temperature up to the Fermi temperature:

$$\tau_e = \frac{1}{A_e T_e^2 + B_l T_l}. \tag{13}$$

On the other hand, the phonon relaxation time τ_l is less temperature sensitive[29]:

$$\tau_l = \frac{3K_l}{C_l V_s^2}. \tag{14}$$

The four thermophysical properties given above are as accurate as known today in the relevant regime of temperatures.

3. Solution Algorithm

The governing equations (2)–(6) for the electron and lattice temperatures are solved with a finite difference method. Since no convective term is involved, a fixed, uniform grid mesh (Fig. 2) is adopted. The spatial derivatives of the electron and lattice temperatures and the heat flux(es) at interior points are approximated with the central difference, and those at the two boundaries are approximated with the forward difference. The temperatures are calculated at the grid points, whereas the heat flux(es) are computed at the halfway point location between two consecutive grid points. At the boundaries the quantities are solved where they are unknown and are directly imposed where they are specified.

In each timestep, the time rates of change of the electron and lattice temperatures, $\dot{T}_e$ and $\dot{T}_l$, are first determined from the energy equations (2) and (4), respectively. The temperatures T_e and T_l are then updated with the forward difference. When the calculated lattice temperature at a grid point reaches the melting point, according to Eq. (5), the lattice temperature remains unchanged until the solid–liquid phase transformation is completed. If the temperature of the superheated liquid at a grid point is equal to or greater than $0.9T_{tc}$, phase explosion is assumed. That grid point, including both the electrons and the metastable liquid, is then eliminated from the model. In case the grid point that undergoes the phase explosion is underneath the surface, those points that locate in front of it are all removed. The associated thermal energy, of course, is also eradicated with the grid point(s). Once the grid point(s) are removed, the insulated boundary condition is imposed to the new surface. With the new temperature fields, the rates of change of the heat fluxes in electrons ($\dot{q}_e$) and the lattice ($\dot{q}_l$) are computed from the microscale constitutive equations (3) and (6), respectively. Subsequently, the heat fluxes q_e and q_l are advanced. Once the current temperatures and heat fluxes in and the new geometry of the target are determined, the above solution procedure repeats for the next timestep.

Since the main purpose of this work is to evaluate the ablation depth, the computation is stopped when phase explosion no longer occurs (i.e., there is not enough thermal energy in the electrons that will be transferred to the metastable liquid to raise the temperature to $0.9T_{tc}$). The checking condition is

$$\int_{T_l}^{T_e} C_e(T)\,\mathrm{d}T \prec \int_{T_l}^{0.9T_{tc}} C_l(T)\,\mathrm{d}T + \rho H_m[1 - u(T_l - T_m)], \tag{15}$$

where u is a unit step function. If the above unequality exists for all the grid points, then phase explosion will no longer take place.

4. Numerical Results and Discussion

The first numerical analysis is conducted for comparing the model calculation of ablation depth with experimental data. The test case is cited from Preuss et al.[21] that a gold film in vacuum is heated by a UV laser beam. The laser pulse width t_p is 500 fs, and the wavelength λ is 248 nm. After that, the effects of laser pulse duration, film thickness, and multiple-pulse laser heating on the material ablation are investigated. The width of the laser pulses considered in the numerical analyses is 500 fs except for those in the

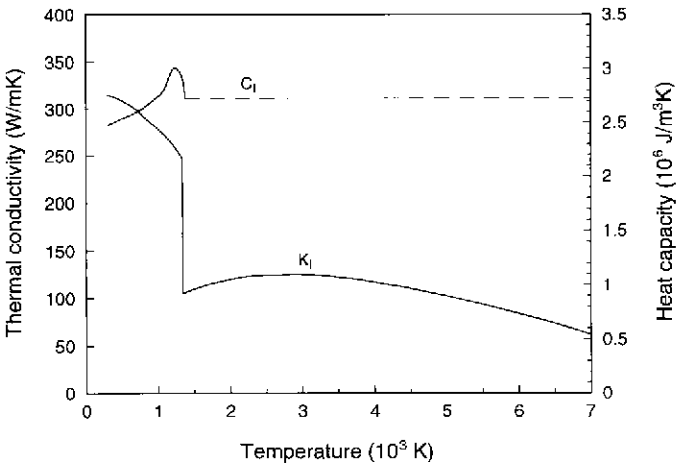

Fig. 3. Thermophyical properties K and C_l of gold.

study of the pulse duration effect. Figure 3 gives the bulk thermal conductivity K of gold[28] and the heat capacity C_l of the gold lattice, where C_l is calculated from the relationship $C = C_e + C_l$ for temperatures below T_b and is assumed to be constant for the temperature beyond T_b as described in the Introduction. The melting, normal boiling, and thermodynamic equilibrium critical temperatures are 1,337, 3,081, and 7,670 K (Ref. 18), respectively. The other thermophysical and optical properties employed are as follows[2,21,22,30,31]: $\rho = 1.93 \times 10^4$ kg/m^3, $C_{eo} = 70$ Jm^{-3}K^{-2}, $G = 8.0 \times 10^{16}$ Wm^{-3}K^{-1}, $K_l = 0$, $R = 0.332$, $\alpha = 14.5$ nm, $\chi = 353$ Wm^{-1}K^{-1}, $\eta = 0.16$, $T_F = 6.42 \times 10^4$ K, $A_e = 1.2 \times 10^7$ K^{-2}s^{-1}, $B_l = 1.23 \times 10^{11}$ K^{-1}s^{-1}, and $H_m = 6.275 \times 10^4$ Jkg^{-1}. The mechanical properties of gold are $E = 74.9$ GPa and $\nu = 0.42$. The electron relaxation time τ_e is 26.3 fs at room temperature and about 0.02 fs at the Fermi temperature according to Eq. (13), and the phonon relaxation time τ_l is 38.7 ps at room temperature according to Eq. (14). For the electron–phonon coupling factor, Wang et al.[31] estimated that the value of G at $k_B T_e = 1$ eV (i.e., $T_e = 1.16 \times 10^4$ K) for gold can increase by a factor of ~6 over the value at room temperature, 2.6×10^{16} Wm^{-3}K^{-1} (Ref. 22). Owing to the fact that the maximum electron temperature studied here is on the order of the Fermi temperature, a larger value of G than that of room temperature is expected. As will be seen, the ablation rate simulated with $G = 8.0 \times 10^{16}$ Wm^{-3}K^{-1} (~3.1 times the value at room temperature) matches very well with the experimental data.

Since the laser pulse width considered here is much longer than the electron relaxation time, especially when the electron temperature is high, the term $\tau_e \partial q_e / \partial t$ in Eq. (3) can be neglected. Numerical analysis, however, showed that a much smaller time increment is needed for the solution convergence if the electron relaxation term is excluded. For that reason, the electron relaxation term is retained in Eq. (3). In the study of the convergence of grid size on the numerical results, three different sizes of grid space, 0.5, 1.0, and 2.0 nm, were examined in the computation of the temperatures and the ablation depth. It was found that a grid size of 1 nm is adequate to resolve the problem. Therefore, uniform-mesh models with the grid size of 1 nm are employed in the following numerical analysis. Figures 4–12 present the results for the single-pulse lasers, while Figs. 13 and 14 present the results for the two consecutive pulses split from a laser beam.

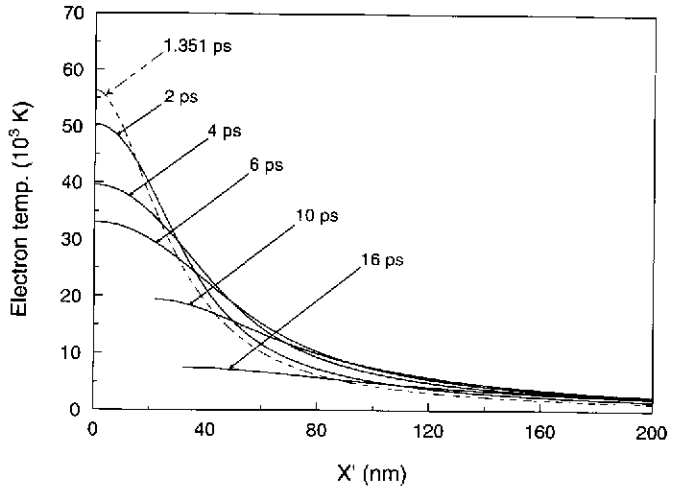

Fig. 4. Electron temperature as a function of distance x' for a 500-nm gold film irradiated by a 500-fs UV laser pulse of $\lambda = 248$ nm and $J_o = 0.4$ J/cm^2, where $x' = L_o - x$, with L_o being the initial film thickness.

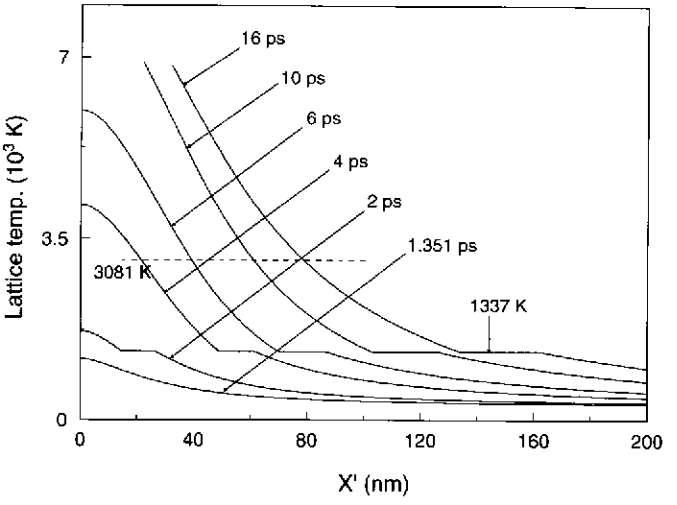

Fig. 5. Lattice temperature as a function of distance x' for a 500-nm gold film irradiated by a 500-fs UV laser pulse of $\lambda = 248$ nm and $J_o = 0.4$ J/cm^2, where $x' = L_o - x$, with L_o being the initial film thickness.

Figure 4 shows the transient electron temperature in a 500-nm gold film as a function of distance x' at different time instants, where $x' = L_o - x$, with L_o denoting the initial film thickness. In this calculation $J_o = 0.4$ J/cm^2. For clarity, only the result for the depth from $x' = 0$ to 200 nm is plotted in Fig. 4. The electron temperature reaches the maximum at $t = 1.351$ ps. The missing portion of the temperature curves for $t = 10$ and 16 ps are the material that is ablated. The lattice temperature distribution is depicted in Fig. 5. As indicated, there are small plateaus on the five temperature curves for $t \geq 2$ ps. These plateaus

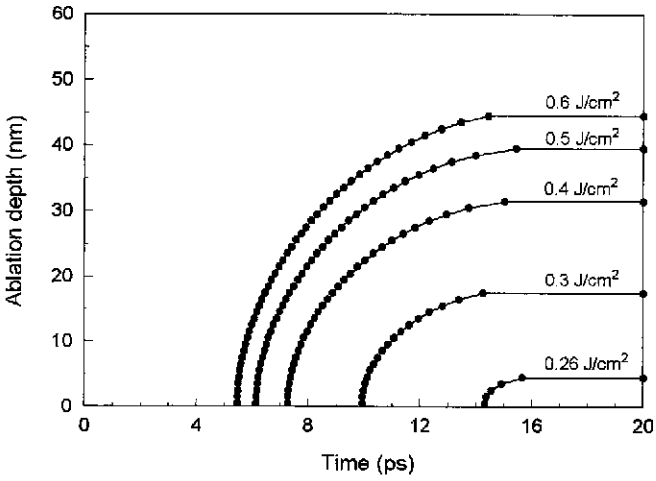

Fig. 6. Time history of the material loss from a 500-nm gold film irradiated by a UV laser pulse of $t_p = 500$ fs and $\lambda = 248$ nm at five laser fluences.

are the interface layer in which the material is undergoing the melting. The right points of the plateaus are where the phase transformation begins, and the left points are where the transformation is completed. The region where the temperature exceeds the normal boiling temperature (3,081 K) is the superheated liquid. For this laser fluence (0.4 J/cm^2), the depth of the superheated liquid is, for example, about 46 nm at $t = 16$ ps.

The time history of material ablation is illustrate in Fig. 6 for five different laser fluences. It appears, as expected, that the higher the laser fluence, the earlier the sputtering starts and the more the material is removed. Note that the laser ablations of the five cases all are completed prior to $t = 16$ ps. The results in Fig. 6 also show that one grid point is removed at a time.

Figure 7 shows the amount of ablated material as a function of laser fluence. The electron–phonon coupling factor at room temperature ($G = 2.6 \times 10^{16}$ Wm^{-3}K^{-1}) was first used in the calculation. As shown in Fig. 7, the simulated results are well off the experimental data.[21] Other values of G were then tested. The results computed with $G = 8.0 \times 10^{16}$ Wm^{-3}K^{-1}, apparently, are in very good agreement with the experimental data except for the region near the ablation threshold. The calculated J_{sh} is about 0.257 J/cm^2, which is slightly higher than the measurement ~0.17 J/cm^2. Another value calculated with the analytical formula[12] is 0.118 J/cm^2. It is worth noting the different dependency of laser fluence for the material ablation. The ablation rate (material removal by an increment of laser fluence) is quite small for the laser fluences lower than ~0.24 J/cm^2, compared to that for the higher fluences. This significant difference implies that material ablation by the lower power laser may not be controlled by phase explosion. Instead, nonthermal damage that is caused by high stresses could be the dominating ablation mechanism.[7,23]

The solid line in Fig. 8 represents the ablation depth obtained from a different approach that includes the heat conduction in the lattice. In this analysis the thermal conductivity given in Fig. 2 is assumed for K_l, and a larger value of G, 1.2×10^{17} Wm^{-3}K^{-1}, is adopted. It is interesting to note that the computed ablation depth does not increase smoothly with the laser fluence; instead, the increase is somewhat snaky. Figure 9 shows the time history of the material loss. For this model, the point-by-point material removal occurs only in

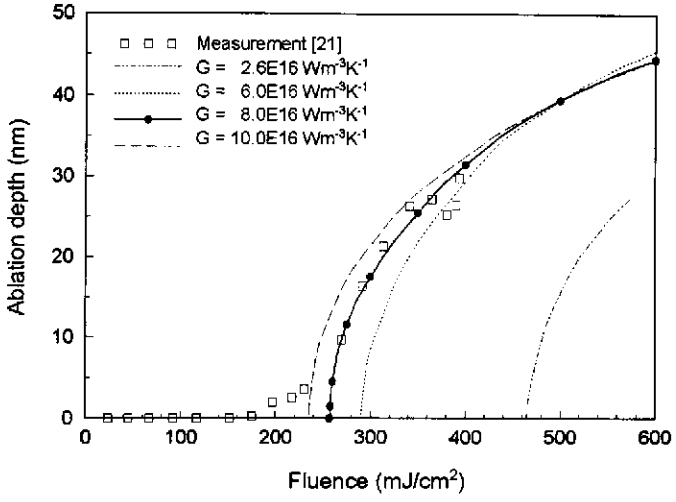

Fig. 7. Sensitivity study of the electron–phonon coupling factor on material ablation for a 500-nm gold film irradiated by a 500-fs UV laser pulse of $\lambda = 248$ nm.

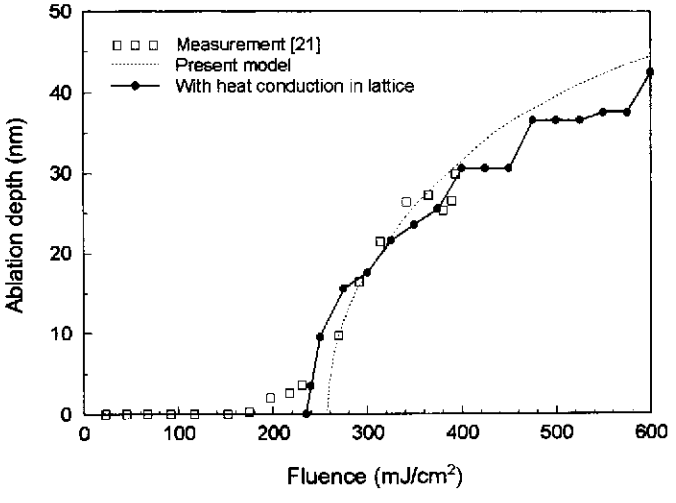

Fig. 8. Comparison of the material ablation behavior simulated with the approaches with and without heat conduction in the lattice.

the beginning of the ablation. After some certain period of time, two or more grid points are removed at a time. This reveals that phase explosion no long occurs at the surface grid point but somewhere beneath the surface. The lattice temperature distribution over the region of $x' = 0$–200 nm is plotted in Fig. 10 for the case of $J_o = 0.4$ J/cm^2. When the heat conduction in the lattice with the phonon relaxation effect is taken into account, the peak lattice temperature would travel from the irradiated surface to inside the material with the speed of thermal wave.[8] Since the superheated liquid explodes from the location where the temperature first reaches the critical point $0.9T_{lc}$, the movement of the peak temperature can explain why the phase explosion occurs at the surface grid point in the early time and shifts to somewhere beneath the surface at the later times. Besides, conduction of the heat

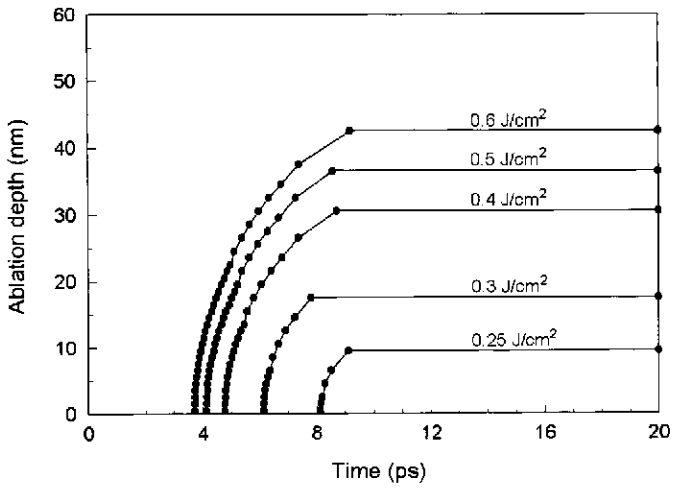

Fig. 9. Time history of the material loss simulated with heat conduction in the lattice.

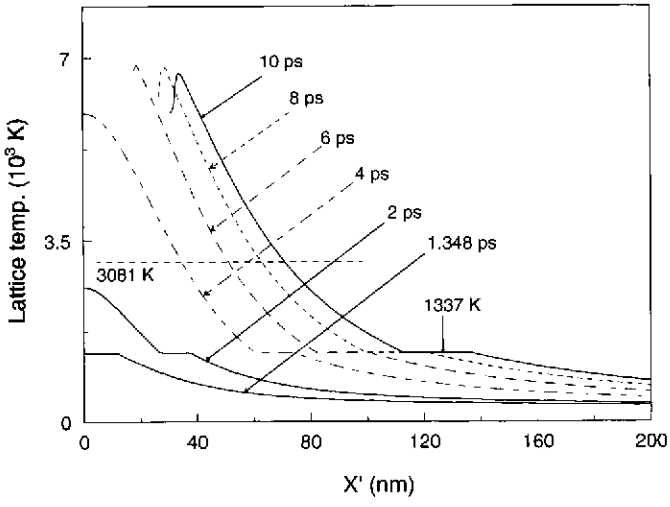

Fig. 10. Lattice temperature as a function of distance x' for a 500-nm gold film irradiated by a 500-fs UV laser pulse of $\lambda = 248$ nm and $J_o = 0.4$ J/cm^2, where $x' = L_o - x$, with L_o being the initial film thickness, simulated with heat conduction in the lattice.

in the lattice from the hot region to the colder one continues to reduce the peak temperature as time lengthens.[8] To make up the conduction loss, more laser power is needed to raise the temperature of the hottest grid point to $0.9T_{tc}$. Accordingly, the amount of ablated material could be the same for two laser pulses unless the fluence of one pulse is greater by a certain amount than the other. Once the hottest grid point (inside the material) explodes, multiple grid points are removed, i.e., there is a sudden jump of the ablation depth. This explains the snaky behavior as seen in Fig. 8. The phase explosion discussed here is a possible phenomenon for materials such as alloys and semiconductor materials, for which the contribution of K_l to K is significant.

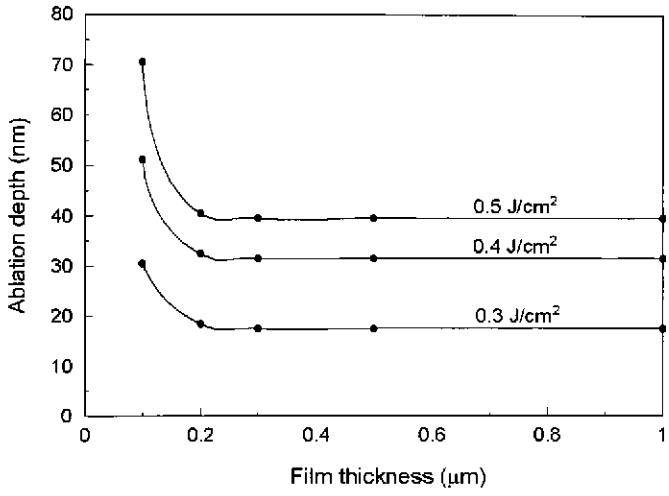

Fig. 11. Effect of film thickness on the ablation depth for gold films heated by a 500-fs UV laser pulse.

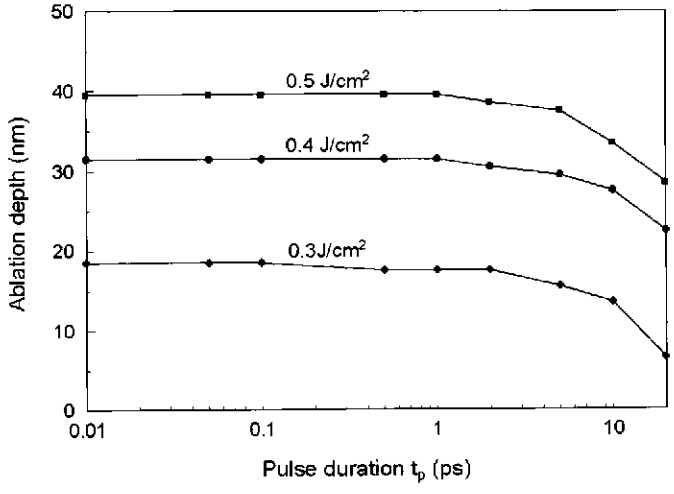

Fig. 12. Effect of laser pulse duration on the material ablation for a gold film heated by UV laser pulses.

The influence of film thickness on the material ablation by ultrashort lasers is shown in Fig. 11. Three laser fluences are studied. It is clearly seen that the calculated ablation depth is independent of the film thickness provided that films are thicker than 300 nm. For films thinner than 300 nm, a higher ablation rate is achieved.

Figure 12 shows the effect of laser pulse length on the material ablation. Nine laser pulse durations, from $t_p = 10$ fs to 20 ps, are examined. In these calculations the same surface reflectivity is assumed. Evidently, the amounts of ablated material are almost identical for the laser pulse durations shorter than a few picoseconds. For longer laser pulses, on the other hand, less material is ablated as the pulse length increases. This confirms that compared

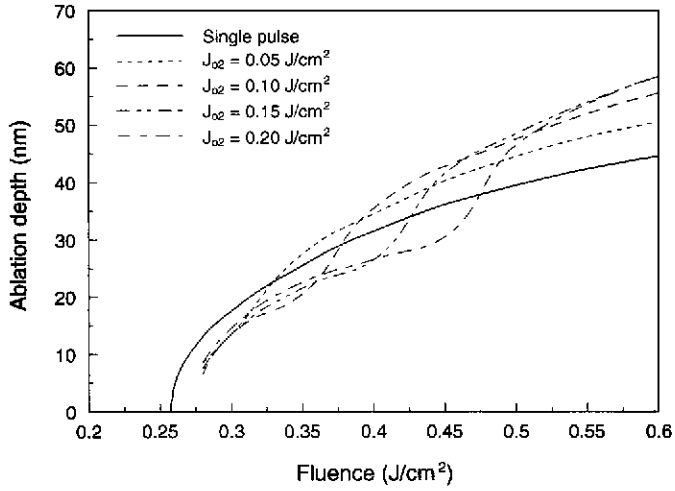

Fig. 13. Influence of the fluence of the second pulse on the ablation depth for a 500-nm gold film heated by the split pulses; $\Delta t = 16$ ps and $J_{o2} = 0.05$, 0.1, 0.15, and 0.2 J/cm^2.

with longer laser pulses, femtosecond lasers need lower fluence to accomplish material ablation.[24]

The lattice temperature distribution shown in Fig. 5 indicates that after laser ablation, a considerable amount of residual thermal energy remains in the superheated liquid. This suggests that ultrafast laser ablation can be optimized if the residual thermal energy is utilized. Therefore, ablation of the gold films by two consecutive pulses split from a laser beam is investigated in this paper. Let J_{o1} and J_{o2} be the laser fluences of the first and second pulses, respectively; thus the total fluence is $J_o = J_{o1} + J_{o2}$. In view of the laser ablations studied above all being completed before $t = 16$ ps (Fig. 6), the separation time Δt of the two split pulses is assumed to be 16 ps. The film used in the analysis is 500 nm thick. Figures 13 and 14 show the influence of the second laser pulse fluence on the amount of ablated material. The fluences of the second pulse presented in Fig. 13 are constant, $J_{o2} = 0.05$, 0.1, 0.15, and 0.20 J/cm^2, while those presented in Fig. 14 vary with the first pulse fluence, $J_{o2} = J_{o1}$ and $J_{o2} = 2J_{o1}$, respectively. As seen in Fig. 13, for the total fluence near the threshold the amount of ablated material by the split pulses is nearly independent of the second pulse fluence. As the total fluence increases, however, the dependency of the second pulse fluence for the material ablation becomes discernible. Interestingly, the total fluence at which the curves of the two split pulses cross the curve of the single pulse is slightly greater than the sum of J_{sh} and J_{o2}. This is also true for the case $J_{o2} = J_{o1}$ (Fig. 14). Although Fig. 14 shows that the case of $J_{o2} = 2J_{o1}$ has a worse performance than that of the single pulse, according to the above statement, the total amount of ablated material should be able to be improved if J_o is at least 0.771 J/cm^2 (the sum of $J_{sh} = 0.257$ J/cm^2 and $J_{02} = 0.514$ J/cm^2). In fact, further analysis finds that the ablation depth is 53.5 nm by a 0.8-J/cm^2 single pulse, for instance, whereas it increases to 56.5 nm by the two split pulses.

The change of the laser ablation result by allocating different energy to the two pulses can be explained as follows. For the total fluence near the threshold, 0.28 J/cm^2 for instance, all the first pulse fluences studied in this work are lower than J_{sh}(= 0.257 J/cm^2). Hence, part of the laser energy of the second pulses is used to continue to heat the material up to the critical

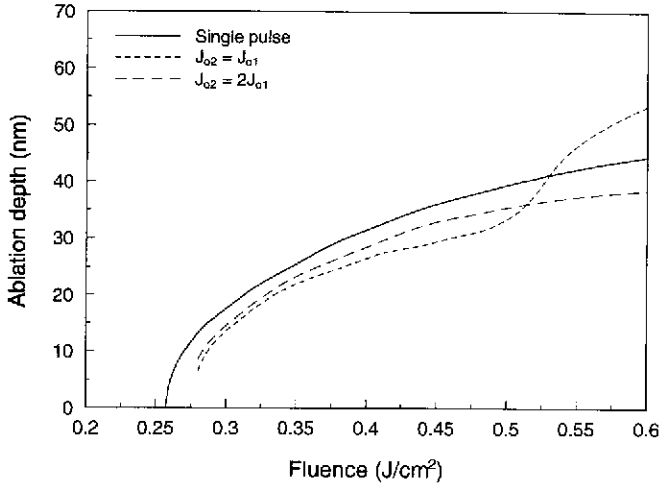

Fig. 14. Influence of the fluence of the second pulse on the ablation depth for a 500-nm gold film heated by the split pulses; $\Delta t = 16$ ps and $J_{o1} \leq J_{o2}$.

temperature ($0.9T_{tc}$). As a result of the similarity of the heating and ablation process to that of a single beam, material ablation by the two split pulses is nearly independent of the energy allocated to the pulses for the same total fluence. The smaller amount of material ablated by the two split pulses than by the single pulse is attributed to the cooling of the superheated liquid during the interruption of the laser energy deposition. For the total fluence much greater than the threshold, in contrast, the first pulse fluence plays an important role in the material ablation. Let us consider the two split pulses whose total power is 350 J/cm^2. For the case of $J_{o2} = 0.05$ J/cm^2, the amount of ablated material by the first pulse ($J_{o1} = 0.3$ J/cm^2) is 17.5 nm. Assuming that the cooling effect is of no consequence, the amount of ablated material by the second pulse can then be estimated with the ablation rate near the threshold. From the ablation result of the single pulse shown in Fig. 13, the ablation rate for the fluence $0.257 \sim 0.307$ J/cm^2 is significantly higher than that for $0.3 \sim 0.35$ J/cm^2. This leads to a larger amount of ablated material, 27.5 vs 25.5 nm by a single pulse. For the other case of $J_{o2} = 0.20$ J/cm^2, no material is removed by the first pulse since $J_{o1} = 0.15$ J/cm$^2 < J_{sh}$. Because of the cooling of the superheated liquid during the interruption of the laser energy deposition, it is impossible for the split pulses to ablate more material than the single pulse. The above discussion draws a conclusion that the first pulse fluence must be greater than the ablation threshold in order to improve energy efficiency of material ablation. It should be pointed out here that the Δt studied in this paper is 16 ps, just a little longer than the completion time of the ablation by the first pulse. If Δt is quite large, the improvement in material ablation would be reduced due to the significant cooling of the superheated liquid.

5. Conclusions

The two-step heating equations along with an isothermal solid–liquid phase transformation are proposed to evaluate the superheating and material ablation of a pure metal irradiated by multiple ultrashort laser pulses. When the temperature of the superheated liquid at a grid point reaches $0.9T_{tc}$, phase explosion is assumed and thus the material point is removed. Good correlation between computations and experimental data on gold films

is achieved through the use of a specific value of the electron–phonon coupling factor. The theoretical model presented in this paper appears capable of defining phase explosion as the dominating mechanism of material ablation of pure metals by high-power, ultrashort-pulse lasers. Failure of the present model to capture the ablation response for the laser power near the ablation threshold is attributed to different ablation mechanisms such as nonthermal damage from high stresses.

The numerical analysis shows that there is an insignificant difference in material ablation response as long as the laser pulse duration is shorter than a few picoseconds. For the longer pulses, the amount of ablated material decreases as the pulse length increases. It is also found that for ultrashort-pulse lasers, the simulated ablation depth is independent of the film thickness provided that gold films are thicker than 300 nm. On the other hand, more material can be ablated for films thinner than 300 nm. In addition, two consecutive pulses split from a high-power, ultrashort-pulse laser beam could improve the ablation performance if the first pulse fluence is greater than the ablation threshold.

References

[1]Anisimov, S.I., B.L. Kapeliovich, and T.L. Perel'man, Sov. Phys. JETP **39**, 375 (1974).

[2]Anismov, S.I., and B. Rethfeld, SPIE **3093**, 192 (1997).

[3]Bulgakova, N.M., and A.V. Bulgakov, Appl. Phys. A **73**, 199 (2001).

[4]Bulgakova, N.M., and I.M. Bourakov, Appl. Surf. Sci. **197–198**, 41 (2002).

[5]Chen, J.K., and J.E. Beraun, Num. Heat Transfer A **40**, 1 (2001).

[6]Chen, J.K., and J.E. Beraun, J. Opt. A: Pure and Appl. Opt. **5**, 168 (2003).

[7]Chen, J.K., J.E. Beraun, L.E. Grimes, and D.Y. Tzou, Int. J. Solids Structures **39**, 3199 (2002).

[8]Chen, J.K., J.E. Beraun, and C.L. Tham, Num. Heat Transfer A (in press) (2003).

[9]Craciun, V., N. Bassim, R.K. Singh, D. Craciun, J. Hermann, and C. Boulmer-Leborgne, Appl. Surf. Sci. **186**, 288 (2002).

[10]Domer, H., and O. Bostanjoglo, Appl. Surf. Sci. **208–209**, 442 (2003).

[11]Dyer, P.E., S.M. Maswadi, and C.D. Walton, Appl. Phys. A **76**, 817 (2003).

[12]Gamaly, E.G., A.V. Rode, B. Luther-Davis, and V.T. Tikhonchuk, Physics Plasmas **9**, 949 (2002).

[13]Huang, H.C., and A.S. Usmani, *Finite Element Analysis for Heat Transfer*, Springer-Verlag, London (1994).

[14]Kelly, R., and A. Miotello, Appl. Surf. Sci. **96–98**, 205 (1996).

[15]Kelly, R., A. Miotello, A. Mele, A.G. Guidoni, J.W. Hastie, P.K. Schuck, and H. Okabe, Appl. Surf. Sci. **133**, 251 (1998).

[16]Lu, Q., S.S. Mao, X. Mao, and R.E. Russo, Appl. Phys. Lett. **80**, 3072 (2002).

[17]Martynyuk, M.M., Soviet Phys. Tech. Phys. **19**, 793 (1974).

[18]Martynyuk, M.M., Russ. J. Phys. Chem. **57**, 494 (1983).

[19]Miotello, A., and R. Kelly, Appl. Phys. A **69S**, S67 (1999).

[20]Momma, C., S. Nolte, B.N. Chichkov, F.V. Alvensleben, and A. Tunnermann, App. Surf. Sci. **109**, 15 (1997).

[21]Preuss, S., A. Demchuk, and M. Stuke, Appl. Phys. A **61**, 33 (1995).

[22]Qiu, T.Q., and C.L. Tien, J. Heat Transfer **115**, 835 (1993).

[23]Schäfer, C., and H.M. Urbassek, Phys. Rev. B **66**, 115404 (2002).

[24]Shirk, M.D., and P.A. Molian, J. Laser Applications **10**, 18 (1998).

[25]Song, K.H., and X. Xu, Appl. Surf. Sci. **127–129**, 111 (1998).

[26]Stuart, B.C., M.D. Feit, S. Herman, A.M. Rubenchik, B.W. Shore, and M.D. Perry, J. Opt. Soc. Am. B **13**, 459 (1996).

[27]Theberge, F., S. Petit, A. Iwasaki, M.R. Kasaai, and S.L. Chin. Appl. Surf. Sci. **191**, 328 (2002).

[28]Touloukian, Y.S., and E.H. Buyco, *Specific Heat, Thermopyhsical Properties of Matter*, Vol. 4. IFI/Plenum, New York (1970).

[29]Tzou, D.Y., *Micro- to Macroscale Heat Transfer*, Taylor and Francis, Washington, DC (1997).

[30]Wagman, D.D., T.L. Jobe, E.S. Domalski, and R.H. Schumn, Temperatures, Pressures, and Heats of Transition, Fusion and Vaporization, in D. E. Gray, (ed.), *American Institute of Physics Handbook*, McGraw–Hill, New York (1972).

[31]Wang, X.Y., R.M. Riffle, Y.S. Lee, and M.C. Downer, Phys. Rev. B **50**, 8016 (1994).
[32]Willis, D.A., and X. Xu, Int. J. Heat Mass Transfer **45**, 3911 (2002).
[33]Xu, X., G. Chen, and K.H. Song, Int. J. Heat Mass Transfer **42**, 1371 (1999).
[34]Xu, X., and K.H. Song, Mater. Sci. Eng. **A292**, 162 (2000).
[35]Zel'dovich, Y.B., and Y.P. Raizer, *Physics of Shock Waves and High-Temperature Hydrodynamic Phenomena*, Academic Press, New York (1967).